Mass Spectrometry Analysis of NMC622/Graphite Li-Ion Cells Electrolyte Degradation Products after Storage and Cycling

Sebastien Rigaud, Ana Cristina Martinez, Tristan Lombard, Sylvie Grugeon, Pierre Tran-Van, Serge Pilard, Stéphane Laruelle

Mass spectrometry analysis of NMC622/graphite Li-ion cells electrolyte degradation products after storage and cycling

Sébastien Rigaud[a], Ana Cristina Martinez[b,c,d], Tristan Lombard[b,c], Sylvie Grugeon[b,c], Pierre Tran-Van[d], Serge Pilard[a], Stephane Laruelle[b,c*]

[a]*Plate-Forme Analytique, Université de Picardie Jules Verne, 33 rue Saint Leu, 80039 Amiens, France*
[b]*Laboratoire de Réactivité et Chimie des Solides, CNRS UMR 7314, Université de Picardie Jules Verne, 33 rue Saint Leu, 80039 Amiens, France*
[c]*Réseau sur le Stockage Electrochimique de l'Energie, CNRS RS2E FR3459, France*
[d]*Renault, DEA-IREB, Technocentre, 1 avenue du Golf, 78288 Guyancourt, France*

[*]*corresponding author: stephane.laruelle@u-picardie.fr*
Tel: +33 322825779

Keywords: PCA, Triton X-100, surfactant, LC-MS, electrolyte degradation, Li-ion battery

Abstract

With the aim of establishing a data simultaneous comparison, the Principal Component Analysis (PCA) statistical tool was applied to $LiNi_{0.6}Mn_{0.2}Co_{0.2}O_2$/graphite Li-ion cells electrolyte's decomposition products detected by UHPLC-ESI-HRMS. Herein, we illustrate how the chemometric tool associated with mass spectrometry data can be relevant to provide information about the presence of unusual molecules. Indeed, pristine Triton X-100 surfactant molecules used in the electrode elaboration process were detected after the impregnation stage. However, as they chemically react and oxidize at a potential lower than 4.5V vs. Li/Li^+, only surfactant derivatives and classical ageing molecules were observed, respectively, after storage and cycling stages at 55°C, leading to a triangle-type correlation circle. On the other hand, global schemes of $LiPF_6$-based electrolyte degradation pathways were elaborated from a comparative study with literature to help interpret results in future electrolyte ageing studies.

Introduction

For over two decades, lithium-ion batteries (LIBs) have been considered as the technology of choice in terms of energy and power for many applications (mobile devices, automotive, stationary, aeronautic, etc.)[1]. Their massive deployment has fostered researchers to ever improve their electrochemical performances[2], while prioritizing sustainable development through environmentally friendly manufacturing processes[3].

Rapidly, endeavours were devoted to restricting the use of organic solvents in the preparation of negative and positive composite electrodes. Polyvinylidene fluoride (PVdF) binder-solubilizing N-methyl-2-pyrrolidone (NMP) suspensions were thus replaced by aqueous slurries consisting of carboxymethyl cellulose (CMC) as binder, black carbon as electron conductive carbon and graphite or $LiFePO_4$ as non-water-reactive negative and positive active materials, respectively. However, the use of a different solvent with other polar and dispersive surface tensions may arise new challenges to overcome, such as particles agglomeration. As the homogeneity of the particles distribution in electrodes is a key parameter for high rate performance, the introduction of surfactants such as sodium dodecyl sulfate (SDS), hexadecyltrimethylammonium bromide (CTAB) and polyethylene glycol p-tert-octyl phenyl ether, commercially called Triton X-100, has been envisaged in slurries to increase particles wettability and thus avoid agglomeration. While the two first surfactants, resp. anionic and cationic, were found to induce deleterious aluminum corrosion[4], the non-ionic amphiphilic Triton X-100 molecule[5,6] with hydrophilic polyethylene oxide chain and hydrocarbon hydrophobic head group proved to favour a more homogeneous carbon black dispersion in both electrodes[7]. However, with a boiling point as high as 270°C, this surfactant may remain in the battery electrodes and likely get dissolved into the electrolyte, which may bring about parasitic electrochemical reactions or makes it trickier post-mortem electrolyte degradation analysis with the presence of unusual molecules.

As an attempt to shed light on the fate of Triton X-100 upon battery functioning, the decision was made to complete the detailed analysis of the electrolyte composition after impregnation and short storage and cycling steps of full Li-ion pouch cell prototypes (Fig. 1). As chromatographic techniques coupled to mass spectrometry analytical tools had demonstrated their benefits for the study of electrolyte mixtures[8], characterizations were performed by making use of ultra-high-performance liquid chromatography-electrospray ionization-high resolution mass spectrometry (UHPLC-ESI-HRMS). Moreover, a multivariate statistical method was employed to assist in processing the mass spectrometry data. The principal component analysis (PCA)[9,10] which was barely utilized in the battery field except for TOF-SIMS[1–3] and operando measurements such as XAS, Mössbauer, and Raman[11–13], helped us provide a simultaneous comparison which brought to light differences between electrolytes from different pouch cell prototypes life steps

Experimental

Pouch cells prototype fabrication. Both single side coated electrodes were laboratory-made. Positive electrodes (4 cm^2) prepared in a dry room (dew point of -58°C) were composed of $LiNi_{0.6}Mn_{0.2}Co_{0.2}O_2$ (NMC622, Umicore) active material (19.3 $mg.cm^{-2}$), conductive carbon black C45 (BET = 45 $m^2.g^{-1}$, 20 nm particle size, Imerys) and PVdF binder (Sigma Aldrich) in a 90/6/4 weight ratio. Negative electrodes (4.84 cm^2) were prepared under ambient air from a slurry containing 91.6 wt.% graphite (Timrex E-SLS30, Ymerys) active material (9.3 $mg.cm^{-2}$), 4 wt.% C45, 4 wt.% CMC (Sigma Aldrich) and 0.4 wt.% Triton-X100 (Sigma Aldrich). Both electrodes were dried at 60°C then calendered to obtain 30-35% porosity. The separator was a 25 µm microporous (55% porosity) polypropylene monolayer membrane (Celgard 2500).

Pouch cells with a capacity of around 14 mAh at 55°C were prepared in the dry room. Three sides were sealed before vacuum-drying cells overnight at 80 ºC. After electrolyte filling (80 µL), the last side was sealed with a vacuum sealer. The electrolyte contained 1M $LiPF_6$ in a 1:1:1 vol. mixture of EC/DEC/EMC (99.9%, H_2O < 20 ppm; Solvionic). Note that the electrolyte volume corresponds to twice the calculated pores volume (electrodes and separator), which is a higher amount compared to that introduced in a commercial 18650 cell (excess ≤20 %).

Pouch cell prototype cycling. Cells were stored in the oven at 25°C for 5h then cycled at 55°C in galvanostatic mode at a rate of C/10 (considering x=1 in $Li_xNi_{0.6}Mn_{0.2}Co_{0.2}O_2$) between 2.8 and 4.3V with a resting time of 10 min. between each charge and discharge sweep. Cycling was performed using a VMP-3 potentiostat/galvanostat (Biologic SA) for 4 and 20 days.

Pouch cell prototype storage. Cells were stored in the oven for 5h then cycled for one cycle and a half, at a rate of C/10 between 2.8 and 4.3V at 25°C. Then, the oven was set at 55°C for 4 and 20 days storage.

Electrolyte recovery from pouch cell prototype. After cycling and/or storage, the cells were introduced into the glove box inside a flask flushed with argon. In the glove box, after opening and dismantling the cell, the separator was put, folded, in a small glass flask and 0.4 mL of acetonitrile (HPLC-MS grade purchased from Biosolve) was added. Vortex stirring for 3 min. was applied to ensure all species from the separator were dissolved. The resulting liquid was diluted 2000 times with acetonitrile of the same grade for UHPLC-ESI-HRMS analysis.

UHPLC-ESI-HRMS analysis. Electrospray high-resolution mass spectrometry experiments (ESI-HRMS) were performed on a hybrid quadrupole time-of-flight instrument (SYNAPT G2-Si, Waters), hyphenated with a UHPLC system (ACQUITY UPLC H-Class). This instrument has an electrospray (ESI) ionization source (Z-spray) and an additional sprayer (Lock Spray)

for the reference compound. UHPLC was performed using an ACQUITY UPLC HSS T3 (100×2.1 mm, 1.8 µm) column from Waters, maintained at 40°C. The elution was performed using a 0.5 mL/min mobile phase gradient of water (A) and acetonitrile (B) both containing 0.1 % formic acid. The gradient used was : (A:B): 100:0 (t = 0 min), 100:0 (t = 2 min), 40:60 (t = 8 min), 40:60 (t = 9 min), 20:80 (t = 11 min), 20:80 (t = 12 min), 100:0 (t = 13 min), 100:0 (t = 17 min). The ESI source was operated in the positive ion mode using a capillary voltage of 3 kV (-2.5 kV in negative ion mode) at the following conditions: cone voltage, 40 V; source offset, 40 V; source temperature, 120°C; desolvation gas temperature, 450°C; desolvation gas flow, 800 L/h, and cone gas flow, 50 L/h. Nitrogen (> 99.5%) was employed as the desolvation and cone gas. Mass calibration was carried out using a sodium formate solution (10mM NaOH in isopropanol/water/formic acid 49.9:49.9:0.2, v/v/v) and Leu-enkephalin (m/z 556.2771) was used as the lock mass solution for accurate mass measurements (1 ng/µL in H_2O/CH_3CN/Formic Acid 50:49.9:0.1, v/v/v). The scan range was m/z 50-1000 at 0.2 s/scan. The TOF was operated in the resolution mode, providing an average resolving power of 25,000 (FWHM). The acquisition was performed with MassLynx software (V4.2, Waters).

Principle component analysis for UHPLC-ESI-HRMS data. For each sample, all base peak intensity (BPI) chromatograms were recorded. The detected ions were characterized by their retention time (tr) and accurate mass (m/z) and then automatically searched and integrated using TargetLynx software (V4.2, Waters). At least one blank per sample was associated with the TargetLynx analysis for the determination of the limit of quantification ($LOQ = \mu_{blanks} + 10*\sigma_{blanks}$) for each m/z at corresponding tr. A threshold of an integration value set at 1000 was then applied to keep only more expressed ions. Lastly, the obtained integration values were formatted as a matrix (column = ions; row = samples) before the importation into SIMCA-P software (V 15.0.2.5959, Umetrics, Sweden) to perform the PCA analysis with univariate scaling. X-axis and y-axis of the biplot of correlation correspond respectively to the principal

components PC1 and PC2 (named [1] and [2]). In this present case, the PC1 is interpreted as the degradation type and PC2, as the degradation progress. The biplots of correlation correspond to an overlay of the score plot and the loadings plot. The score plot is a representation of the observations (samples); the axes are labelled "t". The loading plot is a representation of the variables (ions) as a function of the same principal components; the axes are labelled "p". Lastly, the “corr” label refers to the correlation rescaled, which allows overlaying of “p” and “t” on the same circle of correlation of radius 1. The r^2 displayed on each axis is the percentage of variance explained by each PC (variation in the amount of each ion in all samples). The overall r^2 ($r^2(X)_{tot}$) value corresponds to the sum of r^2 of PC1 and PC2.

Results and discussion

NMC622/Graphite pouch cell prototypes with a capacity of around 14 mAh at 55°C were assembled in the laboratory, according to the protocol described in the experimental section. As Ni-rich layered transition metal oxide active material ($LiNi_{1-x-y}Mn_xCo_yO_2$) may undergo Li^+/H^+ substitution in aqueous solution[14], NMC622 positive electrodes were elaborated from PVdF binder-containing NMP slurries and only negative electrodes were prepared through an aqueous processing with CMC binder and Triton X-100 as dispersing agent. After assembling, all the cells were filled with carbonate-based electrolyte under vacuum then submitted to a resting time of 5 hours at 25°C during which the electrolyte impregnates the electrodes and separator pores (electrolyte sample referred to as T0). After this impregnation period, cells were either stored or cycled at 55°C for 4 or 20 days (electrolyte samples referred to as S4 and S20 or C4 and C20 respectively) (Fig. 1). After each step, cells were opened in a glove box and the electrolyte was extracted from the separator to be analyzed using UHPLC-ESI-HRMS.

Application of PCA on UHPLC-ESI-HRMS data for the study of the electrolyte degradation after impregnation at 25°C or storage and cycling at 55°C. All the ions identified through UHPLC-ESI-HRMS in T0, S4, S20, C4 and C20 electrolyte samples are positioned in the correlation circle of Fig. 2, as a function of the variation of their peak integration value. On this circle of radius 1, each ion is represented by a green point, referred to as variable, and variables are responsible for the positioning of the orange squares, referred to as samples. The correlation between samples or variables depends on the distance on the correlation circle. Strikingly, the impregnated, stored and cycled electrolyte samples do not feature a positive correlation as their variables are arranged into three groups, near the edge of the circle, far away from each other, somehow drawing a triangle.

Basic interpretation of the negative correlation between T0 and S4-S20 samples suggests a substantial chemical evolution of the molecules between steps of impregnation at 25°C and storage at 55°C, as a consequence of thermally driven degradation processes. However, as their variables are located on the same left side, it is assumed that the T0 composition is closer to S4-S20 than C4-C20. On the other hand, one can note that the S20 and C20 samples are nearer the variables, as compared to S4 and C4. As a result of ageing processes, specific molecules concentration (i.e. chromatographic peak area) is expected to increase over storage and cycling time, which could explain these shifts on the correlation circle. Hence, PCA seems an interesting tool that can assist in having a quick overview of the electrolyte degradation extent. These appealing observations given by the graphic representation prompted us to go further into the origin of the chemical evolutions witnessed between the different impregnation, storage and cycling steps.

Analysis of electrolyte samples recovered after impregnation and storage in pouch cell prototypes. The m/z value, associated chemical formula and proposed structure of each ion detected in impregnated (T0) and stored electrolyte samples (S4 and S20) are reported in Table

S1. Surprisingly, all ions belong to three families of oligomers originating from the Triton X-100 surfactant used for the negative electrode elaboration. From calculation, considering the entire surfactant amount introduced in graphite-based slurry remains in the cell, a maximum quantity of 0.2 µmol (concentration of 2.5 $mmol.L^{-1}$) could be contained in pouch cell prototype electrolytes.

The family I is only seen in impregnated electrolyte sample T0. It corresponds to the Triton X-100 oligomers having an isooctylphenylether hydrophobic head group and a chain comprising mainly 6 to 13 ethylene oxide (EO) units and a hydroxyl ending group (Fig. 3a). Triton X-100 proves to be highly reactive at 55°C as this family I is hardly visible in the electrolyte samples after storage for 4 and 20 days. Indeed, S4 and S20 samples only contain modified Triton X-100 oligomers with a fluorophosphate (family II) or a carbonate (family III) ending group instead of hydroxyl (Fig. 3b and 3c). For further quantitative insight into the surfactant chemical evolution, integration values of peaks pertaining to family I, II and III from T0, S4 and S20 samples were reported in Fig. 3.

The presence of family II results from the reaction between the surfactant and the $LiPF_6$ salt-derived molecules. The salt initially reacts with water traces[15,16] to yield POF_3 (Eq. 1) which subsequently undergoes substitution reactions of fluorine in presence of water (Eq. 2) and Triton X-100 oligomers (Eq. 3). Water traces are inevitable. Indeed, even if electrolyte usually contains less than 10 ppm of water, an additional amount is issued from other cell parts as electrodes and separator. Appraisal of water content coming out of the electrolyte-free cell prototypes, at 120°C, was carried out using Karl Fisher titration. 1.5 µmol of water was detected, which would correspond to 0.035 vol.% in the electrolyte. Note that this value is 7.5 times higher than the maximal theoretical amount of surfactant that could remain in the cell.

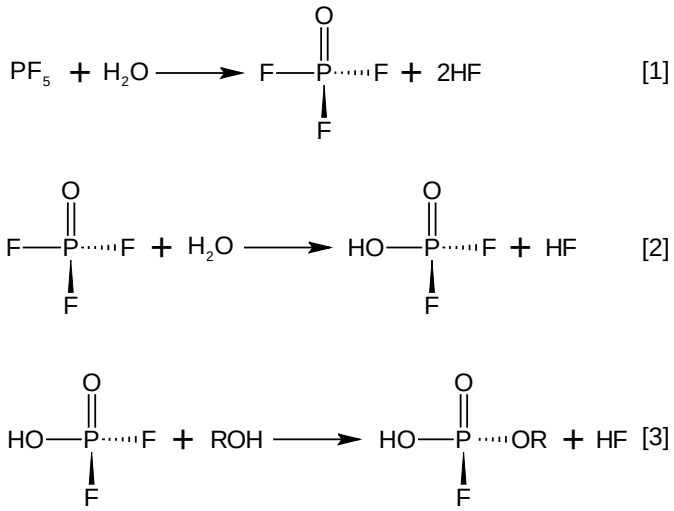

It is worth pointing out that family II is already detected to a lesser extent, in the T0 sample (Fig. 3b), unveiling that the water-initiated reaction is taking place at a temperature as low as 25°C. The presence of this family in both impregnated and stored electrolyte samples thus explains their off-centering in the correlation circle, being placed on the same left side (Fig. 2). To further highlight its impact on their localization, an additional storage test was conducted at 25°C, for 20 days. It was revealed an increased concentration of family II, thus positioning, as expected, the corresponding sample between T0 and S4-S20, as shown in Fig. S1.

Interestingly, family II mostly contains (Fig. 3b) long-chain oligomers with an EO number ranging from 6 to 13. Their concentration levels off between 4 and 20 days of storage at 55°C, as the result of the total consumption of the longer Triton X-100 molecules after 4 days. It is worth noticing that, owing to equivalent concentrations after 4 and 20 days, family II cannot be held responsible for the different localization of S4 and S20 in the correlation circle.

In contrast, family III, detected in S4 and S20 storage samples (Fig. 3c), mostly contains short-chain oligomers ($2<n<5$). This family III results from a transesterification reaction of Triton X-100 molecules with linear alkyl carbonate solvent molecules, EMC or DEC, following Eq. 4.

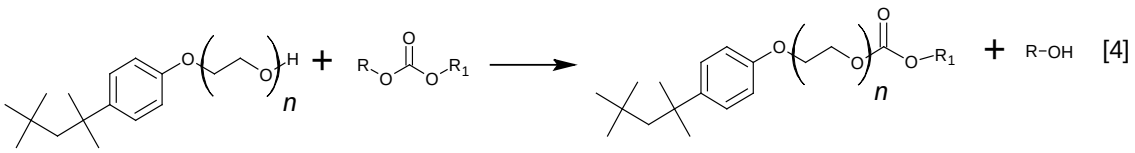

[4]

Unlike the family II, it is not present after the impregnation step at 25°C and its concentration increases between 4 and 20 days of storage at 55°C (Fig. 3c). This concentration rise may be explained by the fact that the shorter-chain Triton X-100 surfactant molecules are less soluble and thus continuously solubilize in the electrolyte even after 4 days. Once solubilized, they immediately react through the transesterification reaction with linear solvent molecules whose quantity is inherently unlimited. Concerning the PCA mining, it can assertively be stated that the increasing concentration of family III upon storage is responsible for the S20 sample shift towards the edge of the correlation circle where the specific storage variables are localized.

In short, the quite intriguing finding that family II mostly contains long-chain oligomers ($6<n<13$) and family III only shorter ones ($2<n<5$) suggests the following selective reactivity; long-chain Triton X-100 oligomers only react with phosphates. Due to their high solubility, the reaction takes place at the very beginning of the storage step, even starting at 25°C. On the contrary, short-chain Triton X-100 molecules only react with solvent molecules, over the entire storage period at 55°C.

Meaningful investigations on thermally driven electrolyte degradation have widely been reported in the literature by several groups. In 2003, Sloop et al.[17] performed storage tests in the 50-85°C temperature range on $LiPF_6$ (1M) in EC/DMC or EC/EMC (1:1 molar ratio) electrolytes. They detected the diethyl (or ethyl methyl or dimethyl) 2,5-dioxahexane dicarboxylate molecules called DEDOHC (or EMDOHC or DMDOHC), and postulated that EC could further undergo a PF_5-assisted polymerization thus yielding poly(ethylene carbonate)s. In 2005, Campion et al.[18] highlighted the production of fluorophosphates and phosphates at 85°C, and also proposed a reaction pathway which remains the reference. The

mechanism implies the substitution reaction of the formed POF_3 with organic carbonates under release of CO_2. Nowak's group also carried out electrolyte storage tests in aluminum flasks at high temperatures up to 95°C, over a maximum period of three weeks. Phosphates, fluorophosphates, poly(ethylene carbonate)s, poly(ethylene oxide)s and their copolymers were identified as a function of the technique and/or the chromatographic column used[19–24].

With respect to the present study, owing to the presence of Triton X-100, none of the above molecules were detected in the electrolyte samples recovered from cells after impregnation or storage for up to 20 days at 55°C. With the aim of getting closer to the literature storage conditions, only electrolyte was introduced in a pouch bag (without cell components) and stored at 55°C for 20 days (ES20 sample in Fig. 1). Some of the molecules reported above were found to be present, namely DEDOHC (m/z of 229.068) and EMDOHC (m/z 215.053), as well as their respective ethylene carbonate oligomers (n=1, m/z 317.084 and m/z 303.068). All of these molecules can be envisaged through a PF_5-assisted transesterification process following Eqs. 5 and 6.

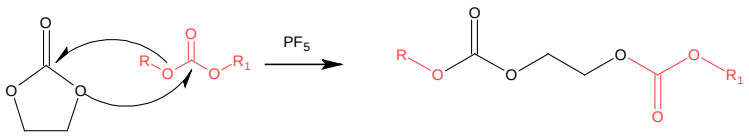

[5]

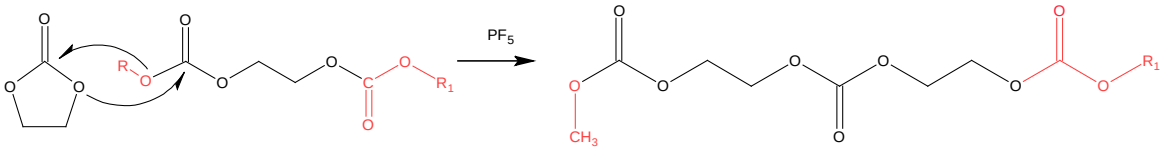

[6]

It is worth noticing that, unlike Nowak's works, no ethylene oxide-based polymers were identified in this sample. As further explained below, it is presumably due to a too low storage temperature that does not allow the triggering of decarboxylation processes. Besides, phosphates and fluorophosphates were not observed in positive mode either. According to the literature[25], only small phosphate-based molecules were usually detected after electrolyte storage, using ionic chromatography or gas chromatography coupled with mass spectrometry.

Assuming the hydrogen of the hydroxyl function is labile, phosphate molecules should possibly be detected through UHPLC-ESI-HRMS in negative mode, which was confirmed through the presence of four molecules reported in Table S2.

Overall, studies dealing with degradation products formed upon storage of carbonate electrolytes and their well-accepted mechanisms were comprehensively reported in the literature. However, the present study, devoted to the analysis of electrolytes recovered from cells, highlights the importance of taking into consideration all components of the batteries when looking into electrolyte reactivity, as any impurities or additives may affect degradation mechanisms. Herein, it is proved that the Triton X-100 oligomers, if remained present in electrodes, solubilize in electrolyte with different kinetics depending on the chain length and selectively react through transesterification reactions with fluorophosphates (Eqs. 1-3) or alkyl carbonates solvents (Eq. 4). Under the study conditions, these reactions turn out to be kinetically favored over transesterification reactions between two carbonate solvent molecules (Eqs. 5 and 6).

Analysis of electrolyte samples recovered after pouch cell prototype cycling at 55°C for 4 and 20 days. Carbonate and phosphate molecules were identified in both samples C4 and C20. The carbonate molecules correspond to DEDOHC, EMDOHC and ethylene carbonate or ethylene oxide oligomers of low molecular mass ($n \leq 2$) with alkyl carbonates ending groups (Table S3 and Fig. 4). Yoshida et al.[26], in 1997, was the first group to observe DEDOHC and EMDOHC as degradation molecules from $LiCoO_2$/graphite cells after cycling (not specified temperature). In their case, as these compounds were found only after the first charge of the cell, the authors proposed reactions were activated by alkoxide anions. Later, in 2005, Sasaki et al.[27] went further into the electrochemically-assisted mechanisms and proposed a two-step nucleophilic substitution mechanism initiated by these anions RO^-, stemming from electrochemical reduction of linear alkyl carbonate solvents. This mechanism involves the formation of the so-

called intermediary A anion and the regeneration of RO^-, following Eqs. 9 and 10. As these DEDOHC and EMDOHC molecules were also detected in electrolyte stored at 55°C for 20 days in pouch bag without cell components (ES20 sample), it can be hypothesized that two reaction mechanism pathways, electrochemically- or PF_5 (thermally favored)-assisted, lead to their formation.

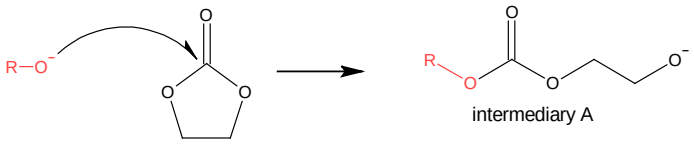

[9]

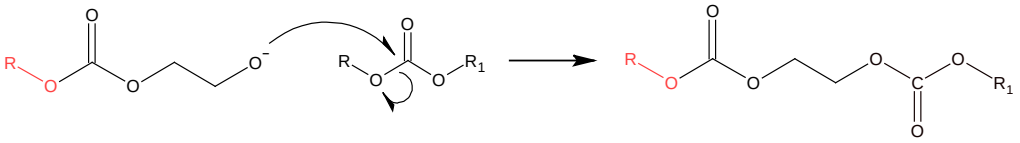

[10]

From 2004[28–31], our group identified ethylene oxide oligomers (with an EO number as high as 9) with either alkyl carbonate/alkyl carbonate, alkyl carbonate/methyl or methyl/methyl ending groups, in EC/DMC 1/1 wt. 1M $LiPF_6$ electrolyte samples recovered from CoO/Li half cells, after long-term cycling at 55°C, as well as from chemical simulation tests conducted at 55°C, in presence of different MeOLi concentrations. To lengthen such EO oligomers, it was assumed that the intermediary A anion can attack the carbon atom of EO (carbon 2 in Fig. 5), leaving lithium alkyl carbonates, as experimentally proved to be precipitated in separator using FTIR[31]. Ethylene carbonate oligomers (with $n \leq 2$) were also detected in some of our investigations[31], resulting from either a PF_5 (thermally favored)-assisted transesterification reaction (Eq. 6) or the attack of the intermediary A anion on the carbon atom of carbonate groups (carbon 1 in Fig. 5) (Eq. 10). Note that, as already mentioned in the storage study, a PF_5-assisted decarboxylation process of these ethylene carbonate oligomers to yield ethylene oxide oligomers is unlikely to occur at such a temperature of 55°C.

Over the last decade, many authors[32,33,24,34,35] have reported the formation of these various degradation compounds upon cycling. Recently, Henschel et al.[20] attempted to clarify the different thermal and electrochemical degradation pathways through LC-HRMS analysis of electrolytes with $^{13}C_3$-labeled EC. They postulated another mechanism for the formation, upon cycling, of ethylene carbonate oligomers with alkyl ether or alkyl carbonate ending functions, involving another initiator than ROLi, the dilithium ethyl monocarbonate, $LiOCH_2CH_2OCO_2Li$ (called LEMC in their paper). The latter would originate from the reduction of two EC molecules to form LEDC (lithium ethylene dicarbonate) followed by a decarboxylation process. These di-lithium salts would attack EC upon elongation process then termination would occur through nucleophilic attack of lithium alkoxide and release of Li_2O to yield neutral oligomers. Accordingly, Li_2O should be present at the interface between electrolyte and SEI (solid electrolyte interphase). However, its presence has not been reported in this area, but rather, nearer the graphite surface[36], raising questions about this new mechanism. Upon storage at 80°C, they propose that the polymerization occurs through an intramolecular rearrangement of EC to form ethylene carbonate oligomers. Similar to Nowak's works reported above, ethylene oxide oligomers as well as ethylene carbonate/ether co-oligomers were also detected and would result from a decarboxylation process. As only ethylene carbonates oligomers were found in our storage study performed at 55°C, it was deduced that the decarboxylation process is occurring only at higher storage temperature, around 80°C, with the assistance of PF_5.

In brief, the mechanism(s) at the origin of the ethylene carbonate and ethylene oxide oligomers seems to highly depend on the cycling temperature. At this temperature of 55°C, it is assumed that ethylene carbonate oligomers found in C4 and C20 electrolyte samples are formed through thermally- and/or electrochemically-assisted reactions whereas ethylene oxide oligomers are originating only from electrochemical reduction reactions (Fig. 5). As shown in Fig. 4, the same carbonate molecules were identified in C4 and C20 and, in accordance with the linear solvents

composition (DEC/EMC), each molecule with ethyl/ethyl carbonate ending groups has its ethyl/methyl counterpart in smaller quantity. Importantly, the concentration of all these carbonate molecules is not greatly affected by the cycle number, increasing only slightly between C4 and C20.

Fluorophosphates, phosphates and diphosphates with mainly alkoxide and ethylene carbonate functions were also identified in these C4 and C20 electrolyte samples recovered after cycling (Table S3). Many studies reported their presence[32–35], and among them, Nowak's group carried out substantial work on their identification. Obviously, the initiating reaction involves $LiPF_6$[37,38,15] following Eq. 11, as demonstrated experimentally by Sloop et al.[17]. Indeed, they showed that half of the solid salt decomposes into PF_5 only after 2 hours at 55°C.

$$LiPF_6 = PF_5 + LiF \qquad [11]$$

Thereafter, this very reactive Lewis acid reacts with water to form phosphoryl fluoride, POF_3, following Eq. 1. The latter undergoes, in turn, nucleophilic substitutions by alkoxides (MeO^- and/or EtO^-) and by Intermediary A anion to yield fluorophosphates (m/z 253.024 et 267.040) or phosphates (m/z 265.043, 279.060 and 293.076). Lengthening of the molecules (m/z 355.055, 367.070 et 381.089) can be envisaged according to Eq. 12:

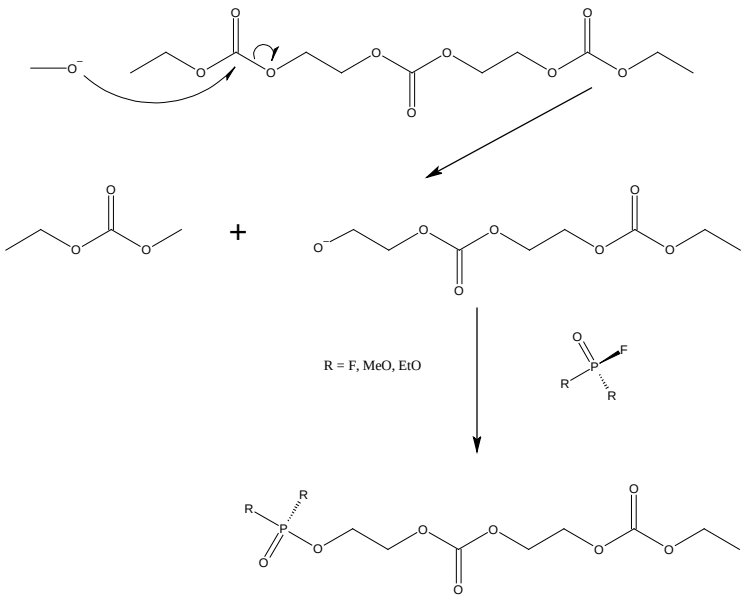

[12]

Note that these proposed phosphates formation pathways (Fig. 6) require the presence of electrochemically-produced anions which explains why these relatively large molecules are only detected after cycling, in positive mode. Unlike carbonates molecules, their concentration increases significantly between 4 and 20 days (Fig. 4), thus making them mostly responsible for the off-centering of the C20 sample towards the edge of the circle.

On the other hand, it can be observed (Table S2, Fig. 4) cyclic phosphate molecules in both storage (m/z 122.985) and cycling (m/z 263.029) samples. EC and H_2O were involved in the chemical reaction mechanism proposed by Webert et al.[39] following Eq. 13.

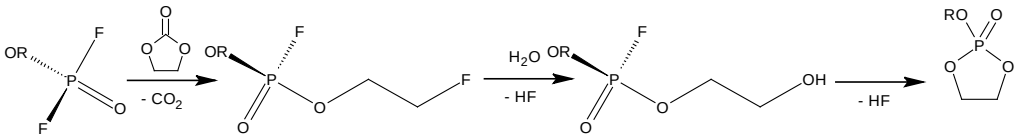

[13]

Regarding diphosphates molecules (Table S3, Fig. 4), both ending groups are linked to one ethylene function, as already detected in many studies. Reaction mechanisms have been proposed by several groups leaving either HF, F^- or both CO_2 and RF as by-products (Eq. 14). Takeda et al.[33] and Henschel et al.[20] suggest that these molecules are produced from a reaction between fluorophosphate and EC as in Eq. 13, while Liu et al.[34,35] propose a reaction between fluorophosphate and the Intermediary A anion (Eq. 9).

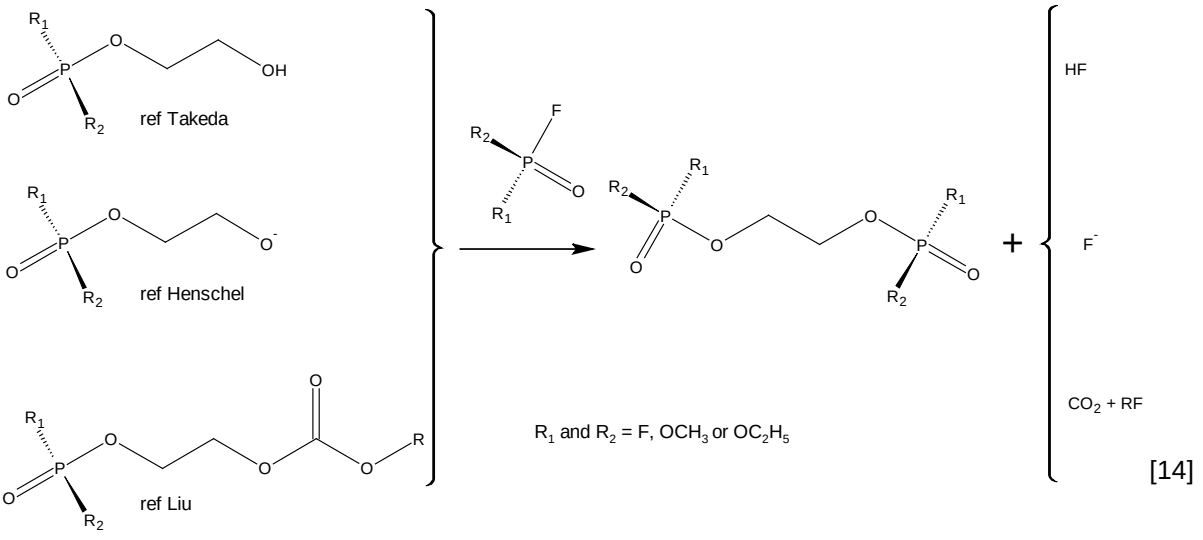

[14]

As shown in Fig. 4, among all phosphate molecules, diphosphates (m/z 317.032 and 331.047) show the largest concentration increase between 4 and 20 days of cycling. This observation makes them interesting molecules to follow while studying the early stages of electrolyte ageing, as they can act as specific indicators of SEI degradation. Knowing that these phosphates are originating from the limited water quantity inside the cell, this statement may not be held after long-term cycling.

In summary, we note that all molecules identified in C4 and C20 electrolyte samples were already observed in the hereabove cited studies and different mechanisms were proposed, suggesting they could be formed from several pathways. Surprisingly, none of the Triton X-100-based molecules previously seen after the impregnation or storage steps (Table S1, Fig. 3) were detected, raising questions about the fate of this surfactant during cycling. Indeed, this molecule consists of an aromatic cycle and EO entities, both being likely to oxidize. To demonstrate its electrochemical activity, a cyclic voltammetry experiment was performed with the electrolyte in which a Triton X-100 molar concentration of 0.2M (way higher than the maximum theoretical surfactant content of 2.5 mM) (Fig. 7a) was added. A platinum disc (2 mm^2) and a piece of lithium were used as working and reference electrodes respectively.

A very large anodic peak is observed between 4.35 and 5.70 V vs. Li/Li^+ which proves the electroactivity of Triton X-100 molecules. Oxidation reactions for the ether functions and the aromatic cycle can be proposed according to Eqs. 15-17.

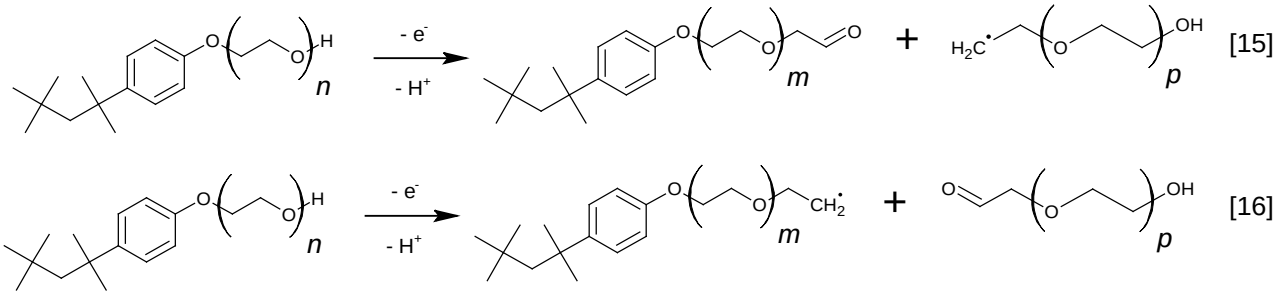

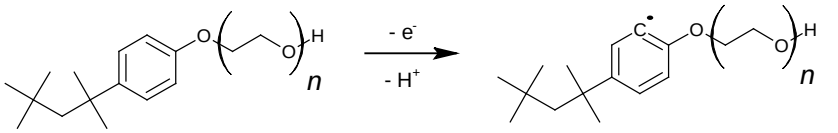

[17]

The oxidation of the ether function yields ethylene glycol oligomers (Eqs. 15-16) whereas the oxidation of the aromatic ring (Eq. 17) would probably trigger a radical polymerization. As ethylene glycol molecules were not detected through the UHPLC-ESI-HRMS analysis of the electrolyte recovered after oxidation, polymers were envisaged to be formed at the surface of the positive electrode, from radical polymerization. It is worth emphasizing that the oxidation potential threshold value obtained on the platinum electrode is higher than the prototype cells' charge cut-off potential value of 4.3V. As this value is dependent on the nature of working electrodes, further cyclic voltammetry experiments were carried out in a Swagelok©-type cell with an NMC622-based tape as working electrode and lithium as both reference and counter electrodes, in the 3.4-4.5V potential range. As shown in Fig. 7b, the first anodic peak between 3.6 and 3.9V characteristic to the delithiation process of NMC622 material, in presence of the electrolyte containing 0.2M Triton X-100, is slightly shifted towards higher potentials (ca. 30 mV), compared to the voltammogram obtained without the surfactant. This shift is due to an increase in polarisation, explained by the higher viscosity of the surfactant concentrated electrolyte. Most importantly, the voltammogram depicts an additional peak between 4.25 and 4.4V vs. Li/Li^+ assigned to the oxidation of the surfactant. Hence, this experimental result suggests that the surfactant is likely to oxidize within the cells cycling potential window (2.8-4.3V), which would explain the disappearance of the triton-based molecules in the electrolyte. Further in-depth investigations would be required to get more insight into the exact oxidation process, for instance, through the chemical composition analysis of the compounds precipitated at the extreme surface of active materials using state-of-the-art surface characterization techniques.

Conclusion

Thanks to the PCA statistical tool, the presence of unusual molecules was conveniently unveiled while analyzing $LiPF_6$-based electrolyte decomposition products using UHPLC-ESI-HRMS.

In the correlation circle, the triangular distribution of the variables pertaining to electrolyte samples recovered after impregnation, storage and cycling was due to the presence of the surfactant, Triton X-100, used for negative electrode tapes manufacturing. Indeed, these surfactant molecules were present in the impregnation sample, however, owing to the thermally favoured reaction kinetic of their alcohol function towards POF_3 and carbonate solvents, all solubilized surfactant oligomers underwent a rapid chemical evolution upon storage at 55°C. On the other hand, as these molecules are also prone to electrochemical oxidation, they were no more detected after cycling; only classical chemical and electrochemical degradation products were observed. In addition, PCA enabled a differentiation between the samples recovered after 4 and 20 days of storage and cycling as the result of a concentration increase of some families (Triton-carbonate in case of storage and phosphates in case of cycling).

With the aim of surveying the ageing of electrolytes recovered from aged Li-ion cells, comprehensive mechanistic schemes of degradation processes were achieved from a comparative study with literature (Figs. 5 and 6). After their thorough examination, it is expected a more linear distribution of variables as function of ageing, as similar compounds, such as ethylene carbonate/oxide oligomers and phosphates, are chemically and/or electrochemically produced throughout the battery lifetime. Their amount will also greatly depend on the internal temperature reached by the battery; i) the thermally-driven SEI dissolution will favour solvents reduction at the origin of the ethylene oxide oligomers and large phosphates formation, ii) because of the thermal degradation of $LiPF_6$ into Lewis acid PF_5, triggering of chemical processes as transesterification and decarboxylation will take place from around 40°C and 80°C respectively, to yield successively ethylene carbonate oligomers and

ethylene oxide oligomers. On the basis of this analysis, PCA tool should be relevant in case of the comparative study of different electrolyte compositions with various SEI-reinforcing additives, solvents or $LiPF_6$ salts substituents.

Acknowledgments: The financial support from the Association Nationale de la Recherche et de la Technologie (ANRT, France) is gratefully acknowledged. The authors thank Michel Armand, Roland Molinié and Grégory Gachot for helpful discussions and advice, and Umicore for NMC cathode materials supply.

References

1. H. Zhang, C. Li, G. G. Eshetu, S. Laruelle, S. Grugeon, K. Zaghib, C. Julien, A. Mauger, D. Guyomard, T. Rojo, N. Gisbert-Trejo, S. Passerini, X. Huang, Z. Zhou, P. Johansson, and M. Forsyth, *Angew. Chem. Int. Ed.*, **59**, 534–538 (2020).

2. C. P. Grey and D. S. Hall, *Nat Commun*, **11**, 6279 (2020).

3. M. Bichon, D. Sotta, N. Dupré, E. De Vito, A. Boulineau, W. Porcher, and B. Lestriez, *ACS Applied Materials & Interfaces*, **11**, 18331–18341 (2019).

4. W. Porcher, B. Lestriez, S. Jouanneau, and D. Guyomard, *Journal of Power Sources*, **195**, 2835–2843 (2010).

5. S. Khabazian, S. Sanjabi, and D. Tonti, *Journal of Industrial and Engineering Chemistry*, **84**, 120–130 (2020).

6. W. Zhang, X. He, W. Pu, J. Li, and C. Wan, *Ionics*, **17**, 473–477 (2011) .

7. X.-M. He, W.-J. Zhang, W.-H. Pu, J.-J. Li, J. Gao, and C.-Y. Jiang, (2011) *Electrode Slurry of Lithium Battery and Electrode of Lithium Battery*, US2011300443 (A1)

8. Y. Stenzel, F. Horsthemke, M. Winter, and S. Nowak, *Separations*, **6**, 26 (2019).

9. C. B. Y. Cordella, *PCA: The Basic Building Block of Chemometrics* I. S. Krull, Editor, InTech, (2012).

10. M. Otto, *Chemometrics: Statistics and Computer Application in Analytical Chemistry, 3rd Edition | Wiley*.

11. D. Muller-Bouvet, N. Emery, N. Tassali, E. Panabière, S. Bach, O. Crosnier, T. Brousse, C. Cénac-Morthe, A. Michalowicz, and J. P. Pereira-Ramos, *Phys. Chem. Chem. Phys.*, **19**, 27204–27211 (2017).

12. M. Fehse, A. Iadecola, M. T. Sougrati, P. Conti, M. Giorgetti, and L. Stievano, *Energy Storage Materials*, **18**, 328–337 (2019).

13. Y. Park, S. Kim, S. Jin, S. Lee, I. Noda, and Y. Jung, *Molecules*, **24**, 291 (2019).

14. A. C. Martinez, S. Grugeon, D. Cailleu, M. Courty, P. Tran-Van, B. Delobel, and S. Laruelle, *Journal of Power Sources*, **468**, 228204 (2020).

15. S. Solchenbach, M. Metzger, M. Egawa, H. Beyer, and H. A. Gasteiger, *J. Electrochem. Soc.*, **165**, A3022–A3028 (2018).

16. S. Wilken, M. Treskow, J. Scheers, P. Johansson, and P. Jacobsson, *RSC Adv.*, **3**, 16359–16364 (2013).

17. S. E. Sloop, J. B. Kerr, and K. Kinoshita, *Journal of Power Sources*, **119–121**, 330–337 (2003).

18. C. L. Campion, W. Li, and B. L. Lucht, *J. Electrochem. Soc.*, **152**, A2327–A2334 (2005).

19. J. Henschel, S. Wiemers-Meyer, M. Diehl, C. Lürenbaum, W. Jiang, M. Winter, and S. Nowak, *Journal of Chromatography A*, **1603**, 438–441 (2019).

20. J. Henschel, C. Peschel, S. Klein, F. Horsthemke, M. Winter, and S. Nowak, *Angew. Chem. Int. Ed.*, **59**, 6128–6137 (2020).

21. J. Menzel, H. Schultz, V. Kraft, J. P. Badillo, M. Winter, and S. Nowak, *RSC Adv.*, **7**, 39314–39324 (2017).

22. C. Peschel, F. Horsthemke, M. Leißing, S. Wiemers-Meyer, J. Henschel, M. Winter, and S. Nowak, *Batteries & Supercaps*, **3**, 1183–1192 (2020).

23. Y. Qian, C. Schultz, P. Niehoff, T. Schwieters, S. Nowak, F. M. Schappacher, and M. Winter, *Journal of Power Sources*, **332**, 60–71 (2016).

24. C. Schultz, S. Vedder, M. Winter, and S. Nowak, *Anal. Chem.*, **88**, 11160–11168 (2016).

25. V. Kraft, W. Weber, M. Grützke, M. Winter, and S. Nowak, *RSC Adv.*, **5**, 80150–80157 (2015).

26. H. Yoshida, T. Fukunaga, T. Hazama, M. Terasaki, M. Mizutani, and M. Yamachi, *Journal of Power Sources*, **68**, 311–315 (1997).

27. T. Sasaki, T. Abe, Y. Iriyama, M. Inaba, and Z. Ogumi, *Journal of Power Sources*, **150**, 208–215 (2005).

28. S. Laruelle, S. Pilard, P. Guenot, S. Grugeon, and J.-M. Tarascon, *Journal of The Electrochemical Society*, **151**, A1202 (2004).

29. L. Gireaud, S. Grugeon, S. Laruelle, S. Pilard, and J.-M. Tarascon, *Journal of The Electrochemical Society*, **152**, A850 (2005).

30. L. Gireaud, S. Grugeon, S. Pilard, P. Guenot, J.-M. Tarascon, and S. Laruelle, *Anal. Chem.*, **78**, 3688–3698 (2006).

31. G. Gachot, S. Grugeon, M. Armand, S. Pilard, P. Guenot, J.-M. Tarascon, and S. Laruelle, *Journal of Power Sources*, **178**, 409–421 (2008).

32. M. Tochihara, H. Nara, D. Mukoyama, T. Yokoshima, T. Momma, and T. Osaka, *J. Electrochem. Soc.*, **162**, A2008–A2015 (2015).

33. S. Takeda, W. Morimura, Y.-H. Liu, T. Sakai, and Y. Saito, *Rapid Commun. Mass Spectrom.*, **30**, 1754–1762 (2016).

34. Y.-H. Liu, S. Takeda, I. Kaneko, H. Yoshitake, M. Yanagida, Y. Saito, and T. Sakai, *RSC Adv.*, **6**, 75777–75781 (2016).

35. Y.-H. Liu, S. Takeda, I. Kaneko, H. Yoshitake, T. Mukai, M. Yanagida, Y. Saito, and T. Sakai, *J. Phys. Chem. C*, **122**, 5864–5870 (2018).

36. S. Malmgren, K. Ciosek, M. Hahlin, T. Gustafsson, M. Gorgoi, H. Rensmo, and K. Edström, *Electrochimica Acta*, **97**, 23–32 (2013).

37. B. Ravdel, K. M. Abraham, R. Gitzendanner, J. DiCarlo, B. Lucht, and C. Campion, *Journal of Power Sources*, **119–121**, 805–810 (2003).

38. E. Zinigrad, L. Larush-Asraf, J. S. Gnanaraj, M. Sprecher, and D. Aurbach, *Thermochimica Acta*, **438**, 184–191 (2005).

39. W. Weber, V. Kraft, M. Grützke, R. Wagner, M. Winter, and S. Nowak, *Journal of Chromatography A*, **1394**, 128–136 (2015).

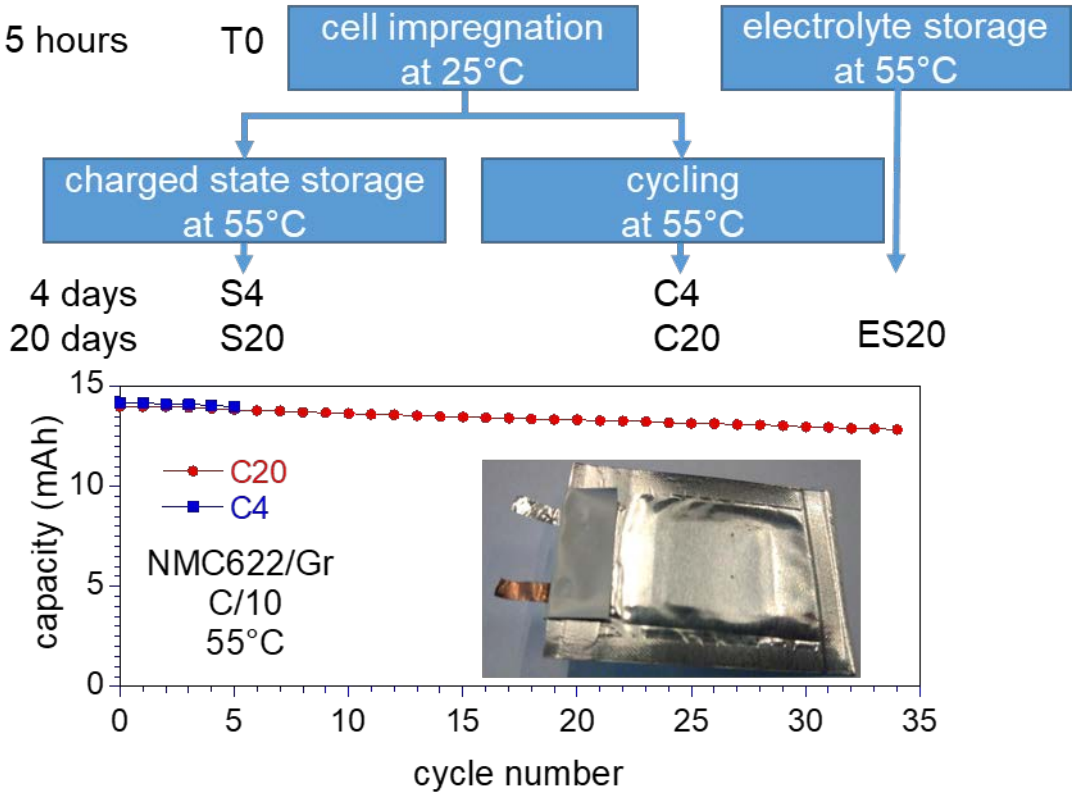
5 hours
T0
cell impregnation at 25°C
electrolyte storage at 55°C
charged state storage at 55°C
cycling at 55°C
4 days
20 days
S4
S20
C4
C20
ES20
capacity (mAh)
cycle number
C20
C4
NMC622/Gr
C/10
55°C

Figure 1

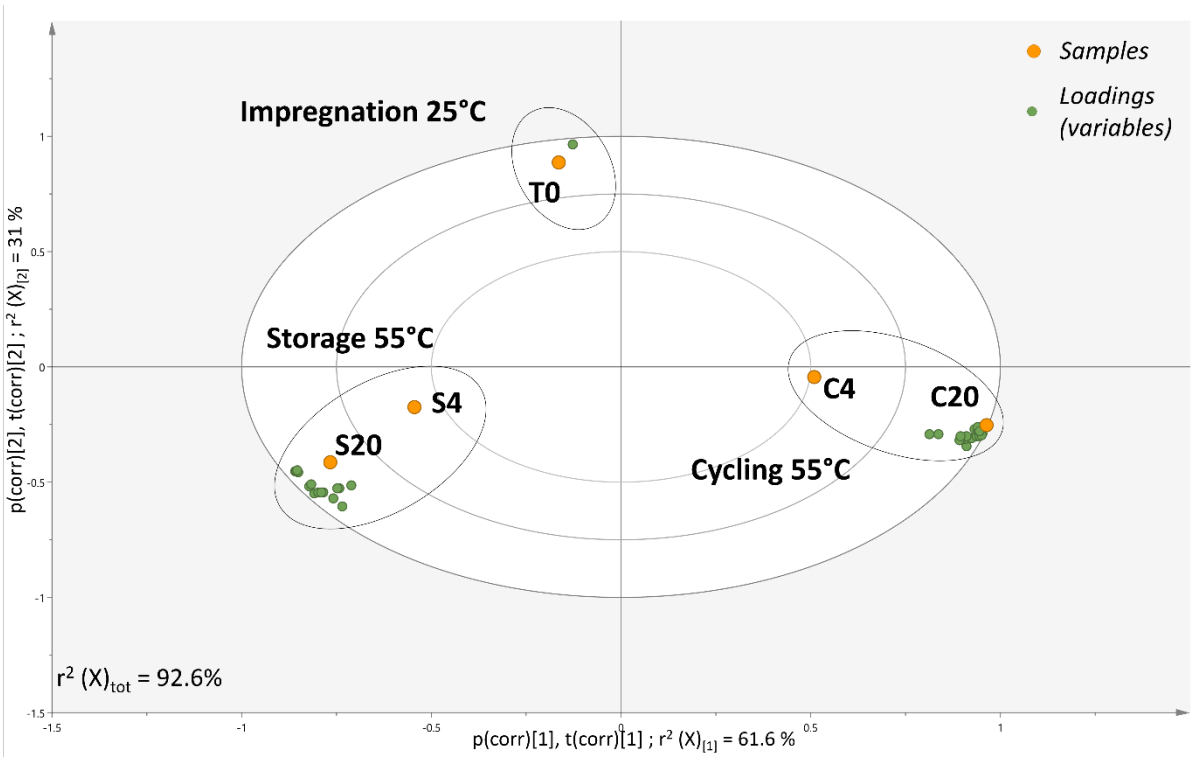
Samples
Loadings (variables)
Impregnation 25°C
T0
Storage 55°C
S4
S20
C4
C20
Cycling 55°C
r² (X)tot = 92.6%
p(corr)[2], t(corr)[2] ; r² (X)[2] = 31 %
p(corr)[1], t(corr)[1] ; r² (X)[1] = 61.6 %

Figure 2

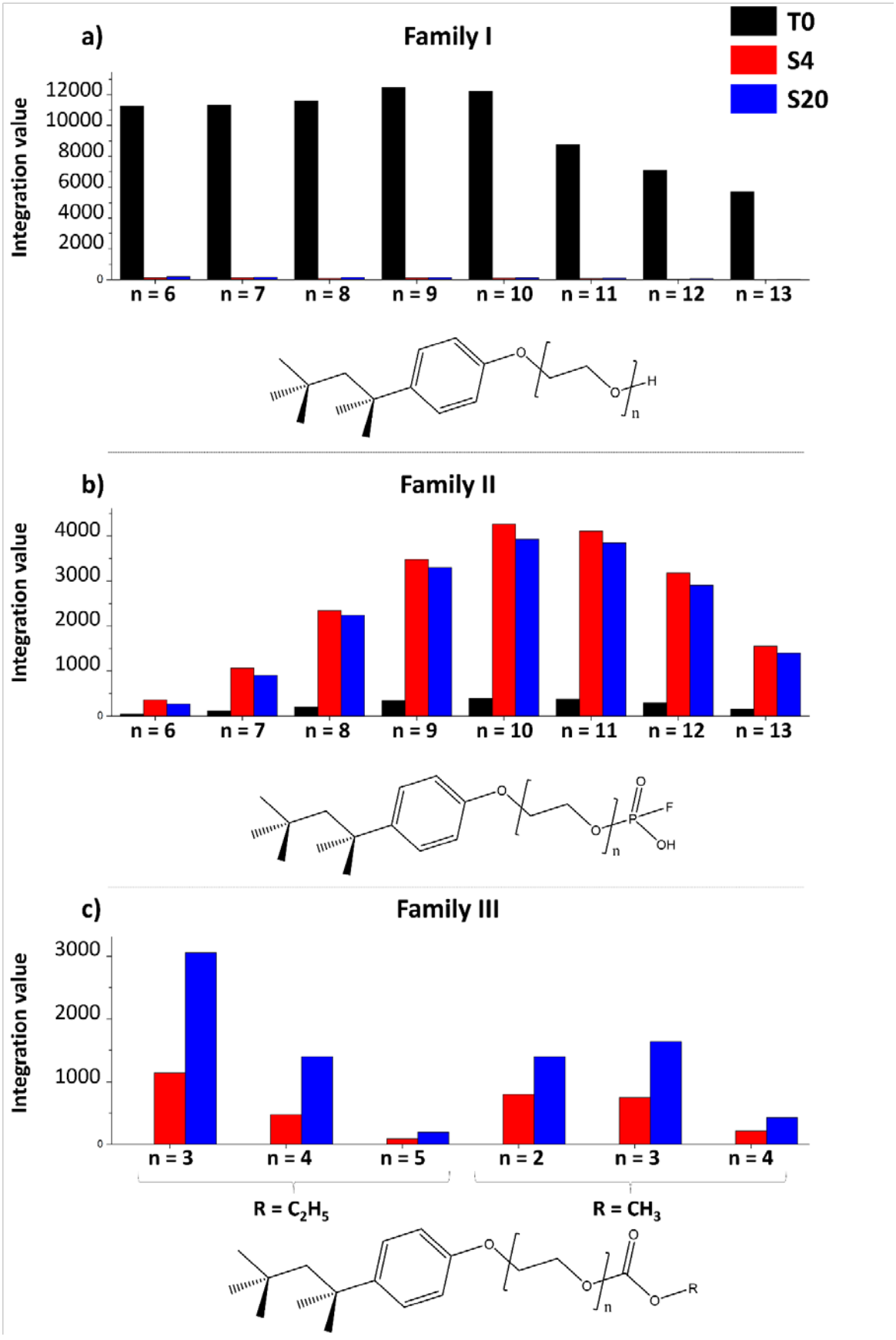
a)
Family I
T0
S4
S20
Integration value
12000
10000
8000
6000
4000
2000
0
n = 6
n = 7
n = 8
n = 9
n = 10
n = 11
n = 12
n = 13
b)
Family II
Integration value
4000
3000
2000
1000
0
n = 6
n = 7
n = 8
n = 9
n = 10
n = 11
n = 12
n = 13
c)
Family III
Integration value
3000
2000
1000
0
n = 3
n = 4
n = 5
n = 2
n = 3
n = 4
R = C2H5
R = CH3

Figure 3

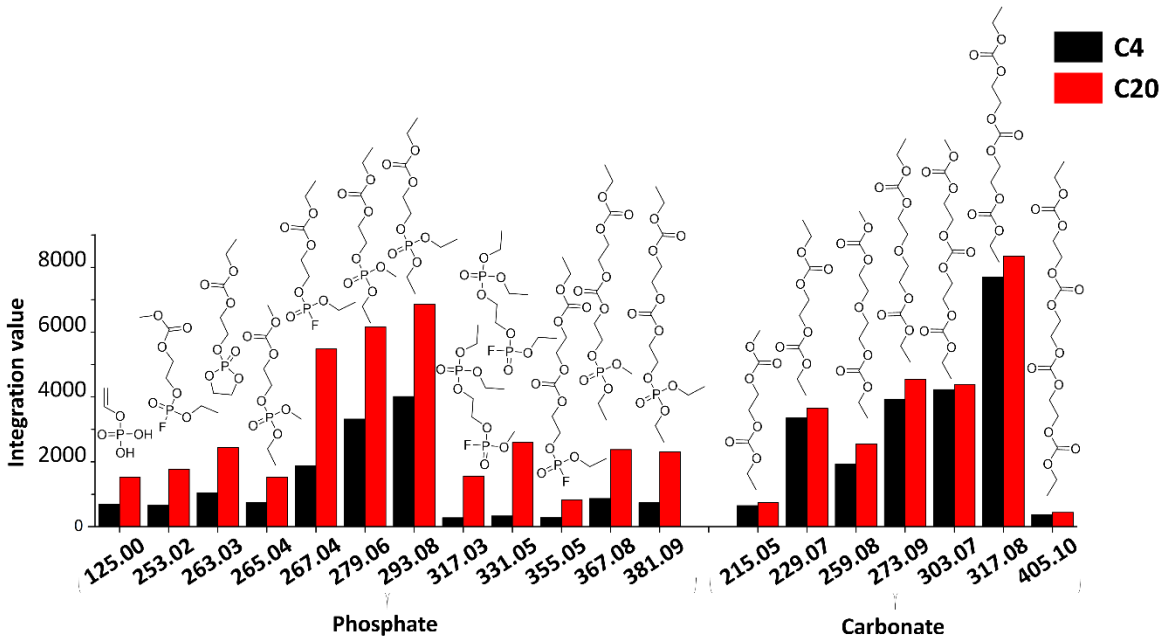
C4
C20
Integration value
8000
6000
4000
2000
0
125.00
253.02
263.03
265.04
267.04
279.06
293.08
317.03
331.05
355.05
367.08
381.09
215.05
229.07
259.08
273.09
303.07
317.08
405.10
Phosphate
Carbonate

Figure 4

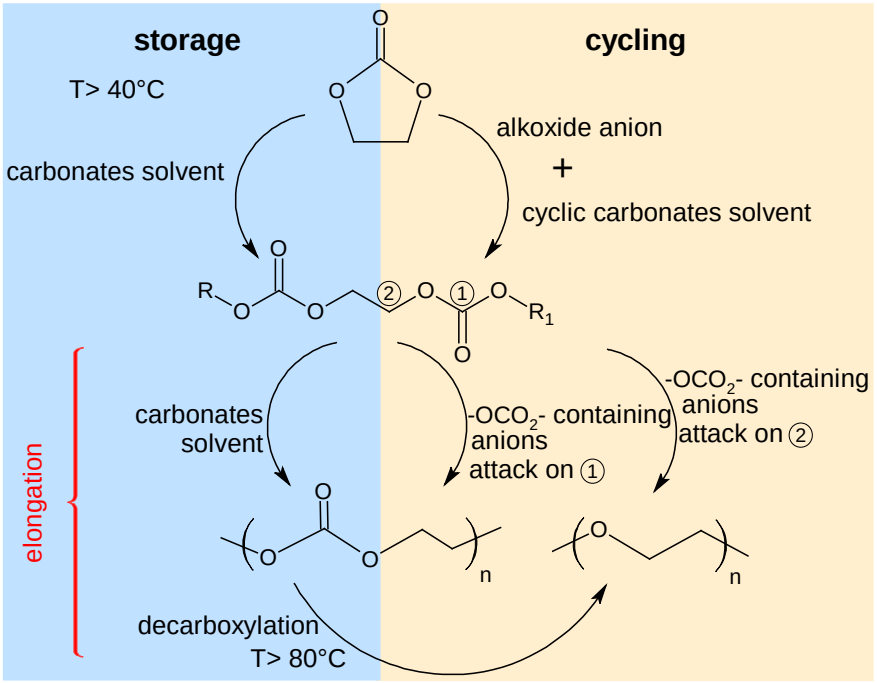
storage
cycling
T> 40°C
carbonates solvent
alkoxide anion
+
cyclic carbonates solvent
carbonates
solvent
-OCO2- containing
anions
attack on ①
-OCO2- containing
anions
attack on ②
elongation
decarboxylation
T> 80°C

Figure 5

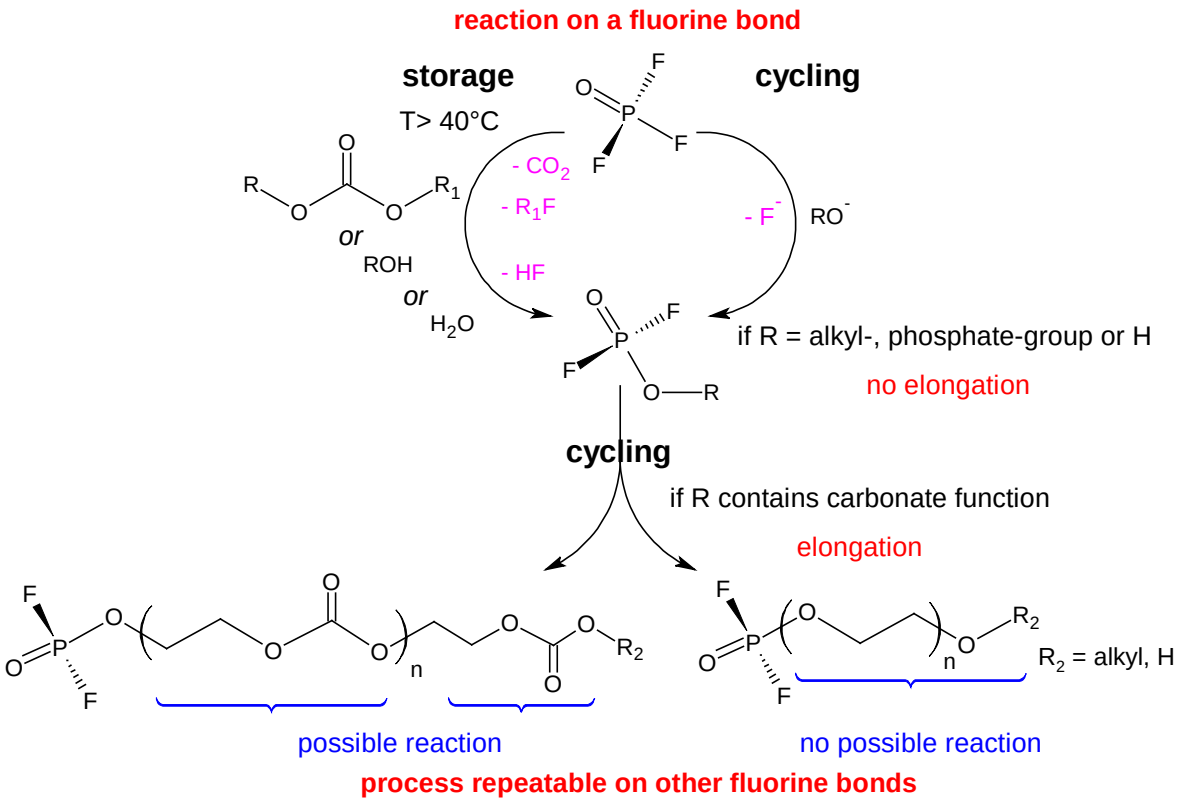
reaction on a fluorine bond
storage
T> 40°C
cycling
- CO2
- R1F
- HF
- F-
RO-
or
ROH
or
H2O
if R = alkyl-, phosphate-group or H
no elongation
cycling
if R contains carbonate function
elongation
R2 = alkyl, H
possible reaction
no possible reaction
process repeatable on other fluorine bonds

Figure 6

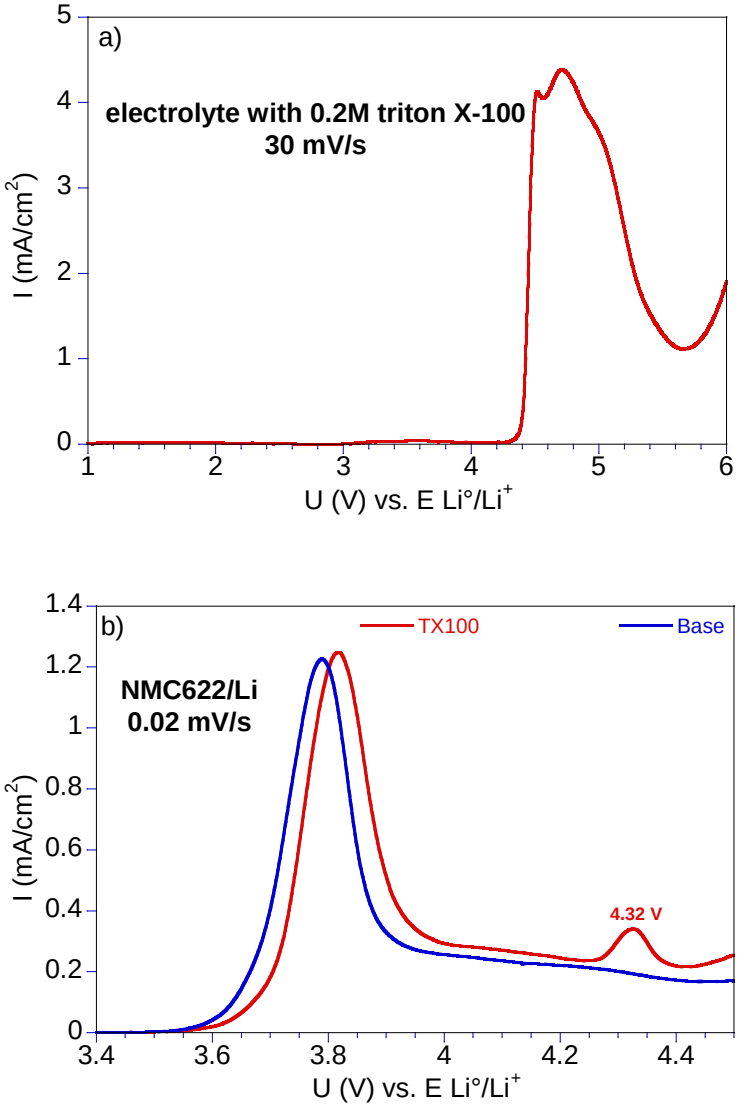
a)
electrolyte with 0.2M triton X-100
30 mV/s
I (mA/cm^2)
U (V) vs. E Li°/Li$^+$
b)
TX100
Base
NMC622/Li
0.02 mV/s
4.32 V
I (mA/cm^2)
U (V) vs. E Li°/Li$^+$

Figure 7

Figure Captions

Figure 1. Electrolyte storage (in a pouch bag without cell components) and pouch cells prototypes impregnation, storage and cycling experiments conditions. Discharge capacity retention of cells corresponding to C4 (6 cycles) and C20 (34 cycles) electrolyte samples.

Figure 2. correlation circle (loadings plot superimposed with score plot) obtained from PCA analysis comprising molecules detected by UHPLC-ESI-HRMS in EC/EMC/DEC 1/1/1 vol. 1M $LiPF_6$ electrolyte recovered after NMC622/graphite pouch cell prototypes impregnation at 25°C (T0), storage (S4, S20) and cycling (C4, C20) at 55°C. With respect to T0, the variables are superimposed leading to only one visible green point.

Figure 3. Integration of UHPLC-ESI-HRMS peaks of electrolyte sample recovered after impregnation at 25°C for 5h (T0, black), storage at 55°C for 4 days (S4, red) and 20 days (S20, blue) for (a) family I (n=6-13), (b) family II (n=6-13) and (c) family III (n=2-5).

Figure 4. Integration of UHPLC-ESI-HRMS peaks of electrolyte sample recovered after cycling at 55°C for 4 days (C4, black) and 20 days (C20, red).

Figure 5. Degradation mechanisms of carbonate solvents under storage and cycling conditions.

Figure 6. $LiPF_6$-mediated degradation mechanisms of carbonate solvents under storage and cycling conditions.

Figure 7. First anodic cyclovoltammetry scan of a) 1M $LiPF_6$ in EC/DEC/EMC (1:1:1 vol.) electrolyte containing 0.2M Triton X-100 using a Pt WE at a rate of 30 mV/s, b) a NMC622/Li half-cell with the same electrolyte with or without 0.2 M Triton X-100 at a rate of 0.02 mV/s.